International Journal of Multidisciplinary and Current Research ISSN: 2321-3124
Research Article Available at: http://ijmcr.com

Design of O-Ring with Outer Sided Restrained Arrangement

S M Muzakkir

Department of Mechanical Engineering, Jamia Millia Islamia, New Delhi, India

Received 06 July 2022, Accepted 05 Aug 2022, Available online 08 Aug 2022, **Vol.10 (July/Aug 2022 issue)**

Abstract

The O-rings are the very commonly employed solution for creating sealing to prevent the loss of pressurized fluid or gases. In the present work the design of an O-ring with outer sided restrain is presented.

Keywords: *Lubricated O-ring, Un-lubricated O-ring, Sealing, Design, Leakage, Elastomers*

1. Introduction

The requirement of sealing is a major concern in the fluid power systems. The sealing is generally provided by the use of O-rings. The O-rings are made up of elastomeric materials. The sealing effect is obtained by the axial or radial compression of O-rings [1]–[7]. There are many designs of O-ring available for different applications. In the present work the design of an O-ring with inner sided restrain is presented.

2. Design of Axially Outer-Sided Restrained O-Ring

The arrangement for the axial outer-sided restrained compression is depicted in figure 1. The groove's nominal outside diameter (mm) is denoted by OD where Bptol and Bntol represent the positive and negative tolerances and ID represents the nominal inner diameter (mm) with positive and negative tolerances as Gptol and Gntol. The groove width (mm) and depth (mm) has been represented by 'W' and 'H' respectively while the clearance between the sealing faces (mm) is represented by 'C'. The design and analysis of the O-ring has been divided into two categories: (i) Unlubricated Condition and (ii) Lubricated Condition depending on whether lubrication was provided to the O-ring prior to its installation within the groove assembly.

3. Unlubricated Condition

The unlubricated condition pertains to the installation of the O-ring inside the assembly without lubrication being provided to its surface. For static applications, where the movement between the sealing faces and the O-ring surface is negligible, unlubricated O-rings do not drastically affect the life of the O-ring.

The cross-sectional diameter plays a crucial role upon the sealing ability of the O-ring. Too small a cross-section makes the O-ring prone to twisting under load leading to leakage while increased cross-section increase the manufacturing costs as well.

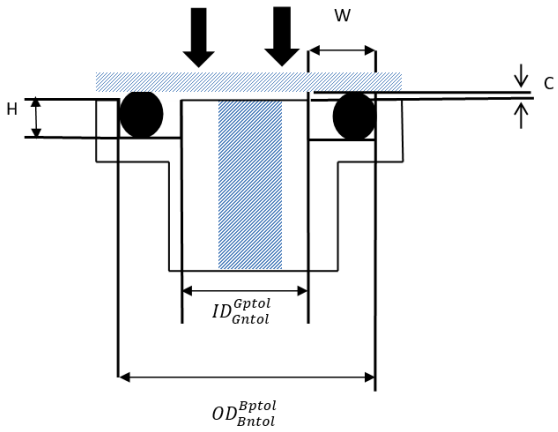

Fig. 1 Axially outer-sided restrained O-ring assembly

In order to optimize the above situation, the handbooks on O-rings provides a range depending upon the range of compression ratio to which the O-ring will be subjected taking into due consideration the various tolerances involved.

The minimum diameter (d_{min}) of the O-ring is decided based on the ratio of groove width to expected minimum compression and the maximum diameter (d_{max}) decided based on the ratio of groove depth (H) to maximum compression. In addition, the clearance and the tolerance are incorporated in estimating the diameter range of the O-ring. The (d_{min}) and (d_{max}) of the O-ring is given by equations (1) and (2) respectively. Where; '*CSptol*' is the positive tolerance on O-ring cross section (mm), '*CSntol*' is the negative tolerance on O-ring cross section (mm), 'C' is the clearance (mm), C_{min} and C_{max} is the minimum and maximum compression of the O-ring.

*Corresponding author's ORCID ID: 0000-0000-0000-0000
DOI: https://doi.org/10.14741/ijmcr.v.10.4.7

$$d_{min} = \frac{H}{1-C_{min}} + CSntol + C \quad (1)$$

$$d_{max} = \frac{H}{1-C_{max}} + CSptol + C \quad (2)$$

The inner diameter (*ID*) of O-ring should be equal to the groove inner diameter. However, the O-ring should be stretched 1 – 5% for proper sealing. By including the tolerances of the groove, the range of ID is estimated form the equation (3) and (4). Where Gntol is the negative tolerance on OD (mm) and IDN is the negative tolerance on O-ring bore (mm).

$$ID_1 = (Gd - Gntol)0.95 + IDN \quad (3)$$

$$ID_2 = (Gd - Gntol)0.99 + IDN \quad (4)$$

Groove Width (GW): The groove width has been calculated taking into consideration the groove depth, the cross-sectional diameter of the O-ring and the inner diameter of the O-ring taking into consideration that the volume of the O-ring should be between 65 to 85 percent of the groove volume. This allows a range for the groove width using Eq. (5) and (6).

$$Groovewidth_1 = \frac{1}{0.65}\left(\frac{\pi^2 d^2 (ID+2d)}{4\left(\pi\left(\frac{OD}{2}-\frac{ID}{2}\right)*\mathrm{H}\right)}\right) - Gntol \quad (5)$$

$$Groovewidth_2 = \frac{1}{0.80}\left(\frac{\pi^2 d^2 (ID+2d)}{4\left(\left(\pi\left(\frac{OD}{2}-\frac{ID}{2}\right)*\mathrm{H}\right)\right)}\right) + Bptol \quad (6)$$

Young's Modulus (E): Two approaches have been suggested for the calculation of Young's Modulus: (i) Using Hardness and (ii) Using Stress-Strain values.

Using Hardness: The estimation for Young's Modulus has been formulated using the value of hardness as a parameter using the empirical relation proposed:

$$E = 0.256 * e^{0.047*(hardness-hardtol)} \quad (7)$$

$$E = 0.256 * e^{0.047*(hardness+hardtol)} \quad (8)$$

Using stress and strain values: The Mooney-Rivlin model has been used, it uses a linear combination of two invariants of the Cauchy-Green deformation tensor in the definition of the stress energy density function (W) which is defined as follows:

$$f = 2(C_2 + C_1\lambda)\left(\lambda - \frac{1}{\lambda^2}\right) \quad (9)$$

Where 'f' denotes the Cauchy stress and C_2 *and* C_1 are material constants. The preference of Mooney-Rivlin model over other models is because it is considered to be the best method for the calculation of Young's Modulus.

Percentage Stretch Range: A limit has been imposed for the stretch of the O-ring for its satisfactory performance. The minimum (Sre_{min}) and maximum (Sre_{max}) stretch is denoted by one minus the ratio of inner diameter of the O-ring to the nominal inner diameter of the groove with its tolerance.

$$Sre\min = 100\left(1 - \frac{ID}{(Gd - Gptol)}\right) \quad (10)$$

$$Sre\max = 100\left(1 - \frac{ID}{(Gd + Gntol)}\right) \quad (11)$$

Groove Height: Groove height is the sum of the groove depth value and clearance and is given by equation (12).

$$h = Groove\,Depth + Clc \quad (12)$$

Initial stress after installation of O-ring inside the assembly: The inner diameter of the O-ring being smaller than that of the groove results in the generation of an initial stretch on the O-ring while installation. If no compressive load is acting upon the ring, the shape of the O-ring has been shown in the figure 2 where the dashed circle represents the initial shape of the O-ring:

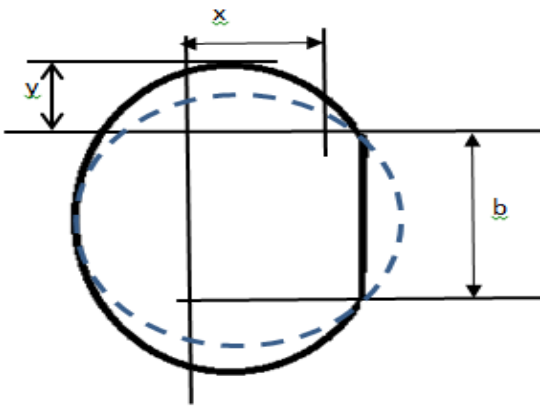

Fig. 2 O-ring deformed shape for one-sided restraint

Where b represents the contact width generated on the lateral wall as a result of initial stretch.

Denoting the initial stretch by δ, the value of the initial stress (σ) is estimated by the following:

$$\sigma_{initial} = E * \delta \quad (13)$$

The load per unit length acting on the O-ring is evaluated as:

$$\frac{L}{dE} = 1.25\delta^{1.5} + 50\,\delta^6 \quad (14)$$

The contact width (b), therefore, as a function of the compressive load is calculated using equation (15).

$$b = \sqrt{\frac{6Ld}{\pi E}} \quad (15)$$

As can be seen in Figure 2, the shape of the O-ring changes to an elliptical shape. This can be divided into the deformed shape into two parts: (i) The left part is a semi-circle having a radius of (r + b/2) while the righthand side can be divided into three parts: a rectangle of area (b*x)

and two quarter ellipses having half axes y and x. This leads to the following:

$$\frac{\pi d^2}{2} = b * x + 2 * (2\pi xy) + \pi\left(y + \frac{b}{2}\right)^2 \quad (16)$$

$$d - \left(y + \frac{b}{2} + x\right) = \delta \quad (17)$$

Solving equation (16) and (17) while taking into consideration equation (15) yields the value of x and y respectively.

Compression in x and y direction: The O-ring is being restrained during compression by one lateral wall of the groove resulting in deformation along the surfaces of the wall. In order to account for this, the compression imposed on the O-ring needs to be normalized taking into due consideration the restraining effects of the lateral walls.

A parameter known as δ_{xy} is defined which is known as the equivalent squeeze in the x direction associated in part due to the force directly applied in the x-direction and in part due to the constraint imposed by the walls which are perpendicular to the x direction i.e. in y direction, which is shown in figure 3. Alternately, for restrained axial loading, δ_{yx} is the equivalent normalized squeeze on the groove walls perpendicular to the top/bottom compressive surfaces as shown.

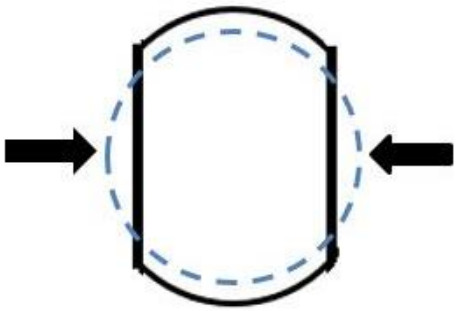

(a) δ_{xy}

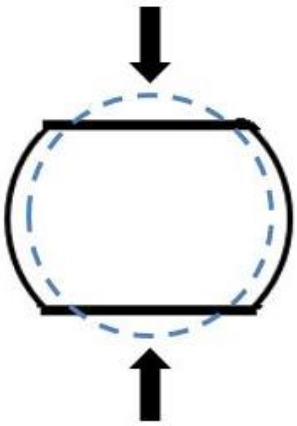

(b) δ_{yx}

Figure 3: Compressive load applied on O-ring

By definition δ_{yx} is estimated as a ratio of difference between (i) a virtual deformed O-ring diameter along the y-axis caused by the compression (δ_{xy}); (ii) the deformed O-ring thickness, *h*. The denominator is the un-deformed O-ring diameter, '*(2y + b)*'. Hence,

$$\delta_{yx} = \frac{(2y+b)f(\delta_{xy}) - h}{(2y+b)} = f(\delta_{xy}) - \frac{h}{(2y+b)} \quad (18)$$

Where;

$$f(\delta) = 1 + 0.415\delta_{yx} + 1.15\delta_{yx}^2 \quad (19)$$

Applying similar reasoning in the perpendicular x-direction, and using the groove width, (as the O-ring thickness), gives the equivalent squeeze

$$\delta_{yx} = \frac{\left(y+\frac{b}{2}+x\right)f(\delta_{xy}) - Groove\ Width}{(y+\frac{b}{2}+x)} = f(\delta_{xy}) - \frac{Groove\ Width}{(y+\frac{b}{2}+x)} \quad (20)$$

Equations (18) and (20) are solved by iterations.

Squeeze after loading: The effective squeeze induced upon the O-ring is calculated from the product of deformation (δ_{xy}) and O-ring diameter (d). The formulation is given in equation (21).

$$squeeze = \delta_{yx} * (2y + b) \quad (21)$$

Load per unit length: The compression load on the O-ring will result in further deformation of the O-ring as a result the compressive load per unit length acting on the O-ring in the y-direction is given by:

$$\frac{L_y}{(2y+b)E} = 1.25{\delta_{yx}}^{1.5} + 50\ {\delta_{yx}}^6 \quad (22)$$

Similarly, the compressive load acting along the x-direction is estimated as:

$$\frac{L_x}{(y+\frac{b}{2}+x)E} = 1.25{\delta_{xy}}^{1.5} + 50\ {\delta_{xy}}^6 \quad (23)$$

Contact Width: The contact width generated between the O-ring and the groove top and bottom surfaces is given by the following expression:

$$Contact\ Width = \sqrt{\frac{6L_y(2y+b)}{\pi E}} \quad (24)$$

Where L_y is the load per unit length multiplied by the deformed chord diameter divided by the Young's Modulus.

Similarly, the contact width generated over the one restrained lateral wall us given by equation (25).

$$Contact\ Trans = \sqrt{\frac{6L_x(y+\frac{b}{2}+x)}{\pi E}} \quad (25)$$

Total compressive Force: After evaluating the load per unit length, the total compressive force exerted by the O-ring will be the product of the load per unit length times the circumference of the O-ring i.e. (π*D).

$$Comp\_Force = \pi * L * D \quad (26)$$

Contact Stress: The stress generated will be distributed over the contact width with its peak at the center and zero just after the edges. Therefore, we need to estimate the value of average stress exerted by the O-ring which is a function of the normalized compression times the Young's Modulus of the material.

$$MaxContStress = \quad (27)$$

$$MaxContStressLat = \left(\frac{4L_x}{\pi\,(Contact\ Trans)}\right) \quad (28)$$

The stress generated will be distributed over the contact width with its maximum at the center of the contact width. The stress generated will be a function of the normalized compression estimated using the least square method. The distribution of the stress is evaluated as follows:

$$P(x) = P_0\sqrt{1 - \left(\frac{2x}{c}\right)^2} \quad (29)$$

Where x represents the distance from the center of the contact width; c represents the contact width and P_0 represents the maximum stress.

The internal fluid sealed by the O-ring will exert pressure on the O-ring, thereby, deforming it further. This consequent deformation will result in increased contact pressure generation by the O-ring. This stress is known as hydro-stress and is expressed as the ratio of the Poisson's ratio divided by one minus the Poisson's ratio times the fluid pressure.

$$Hydrostress = \upsilon * P_1 \quad (30)$$

Therefore, the maximum stress developed by the O-ring becomes:

$$MaxContStress(MPa) = \frac{4L_y}{\pi(contact\ width)} + \upsilon * P_1 \quad (31)$$

$$MaxContStressLat(MPa) = \sigma_{initial} + \left(\frac{4L_x}{\pi\,(Contact\ Trans)}\right) + \upsilon * P_1 \quad (32)$$

4. Lubricated Condition

Lubrication is provided to the O-ring in order to increase the life of the O-ring and reduce the chances of the O-ring from wearing out in any case. But the lubrication provided to the O-ring will result in the increase of the cross-section diameter of the O-ring resulting from permeation of the fluid from the O-ring material. This increased diameter is denoted by d_1 and is dependent on Sw, the percent of swell of the O-ring.

$$d_1 = d\sqrt{1 + 0.01Sw} \quad (33)$$

We proceed with the discussion of the parameters which change as a result of the increase in the cross-sectional radius.

Squeeze for lubricated O-ring after compression

Similar to earlier case of unlubricated condition, the compressed shape of the O-ring as calculated using Eq. (16) and (17) will change with the increase in the O-ring cross-section diameter and therefore, becomes:

$$\frac{\pi d_1^2}{2} = b * x + 2 * (2\pi xy) + \pi\left(y + \frac{b}{2}\right)^2 \quad (34)$$

$$d_1 - \left(y + \frac{b}{2} + x\right) = \delta \quad (35)$$

The normalized squeeze into the O-ring can be calculated as:

$$squeeze = \delta_{yx} * (2y + b) \quad (36)$$

Thereafter, as was the case with unlubricated axially loaded O-rings, the steps involved are quite similar to those for the case with lubricated O-rings.

Conclusion

In the present work, the design of a one-sided restraint O-ring with axial loading where the groove dimensions, hardness, fluid pressure, etc. were provided as inputs was carried out. The O-ring dimensions, contact width, contact stress, peak contact stress and hydro-stress were determined.

References

[1] R. Flitney, *Seals and Sealing Handbook*, Sixth. Butterworth-Heinemann, 2014.

[2] P. Hannifin, *The Parker O-ring Handbook*. Pradifa.

[3] P. Kumar and H. Hirani, "Misalignment effect on gearbox failure: An experimental study," *Meas. J. Int. Meas. Confed.*, vol. 169, no. September 2020, p. 108492, 2021.

[4] K. Ghosh, S. Mazumder, B. Kumar Singh, H. Hirani, P. Roy, and N. Mandal, "Tribological Property Investigation of Self-Lubricating Molybdenum-Based Zirconia Ceramic Composite Operational at Elevated Temperature," *J. Tribol.*, vol. 142, no. 2, pp. 1–8, 2020.

[5] P. Kumar, H. Hirani, and A. Agrawal, "Fatigue failure prediction in spur gear pair using AGMA approach," *Mater. Today Proc.*, vol. 4, no. 2, pp. 2470–2477, 2017.

[6] K. P. Lijesh, D. Kumar, and H. Hirani, "Effect of disc hardness on MR brake performance," *Eng. Fail. Anal.*, vol. 74, pp. 228–238, 2017.

[7] K. P. Lijesh and H. Hirani, "Design and Development of Permanent Magneto-Hydrodynamic Hybrid Journal Bearing," *J. Tribol.*, vol. 139, no. 4, 2017.

[8] K. P. Lijesh, D. Kumar, and H. Hirani, "Synthesis and field dependent shear stress evaluation of stable MR fluid for brake application," *Ind. Lubr. Tribol.*, vol. 69, no. 5, pp. 655–665, 2017.

[9] K. P. Lijesh, D. Kumar, S. M. Muzakkir, and H. Hirani, "Thermal and frictional performance evaluation of nano lubricant with

multi wall carbon nano tubes (MWCNTs) as nano-additive," *AIP Conf. Proc.*, vol. 1953, no. May, pp. 1–6, 2018.
[10] P. Kumar, H. Hirani, and A. K. Agrawal, "Online condition monitoring of misaligned meshing gears using wear debris and oil quality sensors," *Ind. Lubr. Tribol.*, vol. 70, no. 4, pp. 645–655, 2018.
[11] P. Kumar, H. Hirani, and A. Kumar Agrawal, "Effect of gear misalignment on contact area: Theoretical and experimental studies," *Measurement*, vol. 132, pp. 359–368, Jan. 2019.
[12] P. Kumar, H. Hirani, and A. Kumar Agrawal, "Effect of gear misalignment on contact area: Theoretical and experimental studies," *Meas. J. Int. Meas. Confed.*, vol. 132, pp. 359–368, 2019.
[13] P. Kumar, H. Hirani, and A. K. Agrawal, "Modeling and Simulation of Mild Wear of Spur Gear Considering Radial Misalignment," *Iran. J. Sci. Technol. - Trans. Mech. Eng.*, vol. 43, pp. 107–116, 2019.
[14] H. Hirani, T. V. V. L. N. Rao, K. Athre, and S. Biswas, "Rapid performance evaluation of journal bearings," *Tribol. Int.*, vol. 30, no. 11, pp. 825–834, 1997.
[15] H. Hirani, "Theroretical and Experimental Studies on Design of Dynamically Loaded Journal Bearing," 1998.
[16] H. Hirani, K. Athre, and S. Biswas, "Rapid and globally convergent method for dynamically loaded journal bearing design," *Proc. Inst. Mech. Eng. Part J J. Eng. Tribol.*, vol. 212, no. 3, pp. 207–213, 1998.
[17] H. Hirani, K. Athre, and S. Biswas, "Length Journal Bearings : Analytical Method of Solution," *J. Tribol.*, vol. 121, no. October, 1999.
[18] H. Hirani, K. Athre, and S. Biswas, "Dynamic analysis of engine bearings," *Int. J. Rotating Mach.*, vol. 5, no. 4, pp. 283–293, 1999.
[19] H. Hirani, K. Athre, and S. Biswas, "Comprehensive design methodology for an engine journal bearing," *Proc. Inst. Mech. Eng. Part J J. Eng. Tribol.*, vol. 214, no. 4, pp. 401–412, 2000.
[20] T. V. V. L. N. Rao, S. Biswas, H. Hirani, and K. Athre, "An analytical approach to evaluate dynamic coefficients and nonlinear transient analysis of a hydrodynamic journal bearing," *Tribol. Trans.*, vol. 43, no. 1, pp. 109–115, 2000.
[21] H. Hirani, K. Athre, and S. Biswas, "A Hybrid Solution Scheme for Performance Evaluation of Crankshaft Bearings," *J. Tribol.*, vol. 122, no. October, pp. 733–740, 2000.
[22] H. Hirani, K. Athre, and S. Biswas, "A Simplified Mass Conserving Algorithm for Journal Bearing under Large Dynamic Loads," *Int. J. Rotating Mach.*, vol. 7, no. 1, pp. 41–51, 2001.
[23] H. Hirani, K. Athre, and S. Biswas, "Lubricant shear thinning analysis of engine journal bearings," *Tribol. Trans.*, vol. 44, no. 1, pp. 125–131, 2001.
[24] R. K. Burla, P. Seshu, H. Hirani, P. R. Sajanpawar, and H. S. Suresh, "Three dimensional finite element analysis of crankshaft torsional vibrations using parametric modeling techniques," *SAE Tech. Pap.*, no. March 2020, 2003.
[25] H. Hirani and T. V. V. L. N. Rao, "Optimization of Journal Bearing Groove Geometry Using Genetic Algorithm," *NaCoMM03, IIT Delhi, India*, vol. 1, pp. 1–9, 2003.
[26] H. Hirani, "Multiobjective optimization of a journal bearing using the Pareto optimality concept," *Proc. Inst. Mech. Eng. Part J J. Eng. Tribol.*, vol. 218, no. 4, pp. 323–336, 2004.
[27] H. Hirani and P. Samanta, "Performance evaluation of magnetohydrodynamic bearing," *Proc. World Tribol. Congr. III - 2005*, pp. 97–98, 2005.
[28] H. Hirani and P. Samanta, "Test setup for magneto hydrodynamic journal bearing," in *NaCoMM-2005*, 2005, pp. 298–303.
[29] H. Hirani and N. P. Suh, "Journal bearing design using multiobjective genetic algorithm and axiomatic design approaches," *Tribol. Int.*, vol. 38, no. 5, pp. 481–491, 2005.
[30] H. Hirani, "Multiobjective optimization of journal bearing using mass conserving and genetic algorithms," *Proc. Inst. Mech. Eng. Part J J. Eng. Tribol.*, vol. 219, no. 3, pp. 235–248, 2005.
[31] P. Samanta and H. Hirani, "A simplified Optimization Approach for Permanent Magnetic Journal Bearing," *Indian J. Tribol.*, vol. 2, no. 2, pp. 23–28, 2007.
[32] H. Hirani and P. Samanta, "Hybrid (hydrodynamic + permanent magnetic) journal bearings," *Proc. Inst. Mech. Eng. Part J J. Eng. Tribol.*, vol. 221, no. 8, pp. 881–891, 2007.
[33] V. K. Sukhwani and H. Hirani, "Synthesis and characterization of low cost magnetorheological (MR) fluids," *Behav. Mech. Multifunct. Compos. Mater. 2007*, vol. 6526, p. 65262R, 2007.
[34] H. Hirani and C. S. Manjunatha, "Performance evaluation of a magnetorheological fluid variable valve," *Proc. Inst. Mech. Eng. Part D J. Automob. Eng.*, vol. 221, no. 1, pp. 83–93, 2007.
[35] P. Samanta and H. Hirani, "Magnetic Bearing Configurations: Theoretical and Experimental Studies," *IEEE Trans. Magn.*, vol. 44, no. 2, pp. 292–300, Feb. 2008.
[36] V. K. Sukhwani and H. Hirani, "Design, development, and performance evaluation of high-speed magnetorheological brakes," *Proc. Inst. Mech. Eng. Part L J. Mater. Des. Appl.*, vol. 222, no. 1, pp. 73–82, 2008.
[37] V. K. Sukhwani and H. Hirani, "A Comparative Study of Magnetorheological-Fluid-Brake and Magnetorheological-Grease-Brake," *Tribol. Online*, vol. 3, no. 1, pp. 31–35, 2008.
[38] H. Hirani and S. S. Goilkar, "Tribological Characterization of Carbon Graphite Secondary Seal," *Indian J. Tribol.*, vol. 4(2), pp. 1–6, 2009.
[39] H. Hirani and S. S. Goilkar, "Formation of transfer layer and its effect on friction and wear of carbon-graphite face seal under dry, water and steam environments," *Wear*, vol. 266, no. 11–12, pp. 1141–1154, 2009.
[40] S. S. Goilkar and H. Hirani, "Design and development of a test setup for online wear monitoring of mechanical face seals using a torque sensor," *Tribol. Trans.*, vol. 52, no. 1, pp. 47–58, 2009.
[41] H. Hirani and M. Verma, "Tribological study of elastomeric bearings for marine propeller shaft system," *Tribol. Int.*, vol. 42, no. 2, pp. 378–390, 2009.
[42] H. Hirani, "Root cause failure analysis of outer ring fracture of four-row cylindrical roller bearing," *Tribol. Trans.*, vol. 52, no. 2, pp. 180–190, 2009.
[43] H. Hirani, "Online Wear monitoring of Spur Gears," *Indian J. Tribol.*, vol. 4(2), pp. 38–43, 2009.
[44] S. S. Goilkar and H. Hirani, "Parametric study on balance ratio of mechanical face seal in steam environment," *Tribol. Int.*, vol. 43, no. 5–6, pp. 1180–1185, 2010.
[45] H. Hirani and S. S. Goilkar, "Rotordynamic Analysis of Carbon Graphite Seals of a Steam Rotary Joint," in *IuTAM Symposium on Emerging Trends in Rotor Dynamics*, 2011, pp. 253–262.
[46] S. Gupta and H. Hirani, "Optimization of magnetorheological brake," *Am. Soc. Mech. Eng. Tribol. Div. TRIB*, pp. 405–406, 2011.
[47] S. Verma, V. Kumar, and K. D. Gupta, "Performance analysis of flexible multirecess hydrostatic journal bearing operating with micropolar lubricant," *Lubr. Sci.*, vol. 24, no. 6, pp. 273–292, 2012.
[48] H. Hirani, "Online Condition Monitoring of High Speed

Gears Using Vibration and Oil Anlyses," in *Thermal, Fluid and Manufacturing Sciences*, New Delhi: Narosa publishing House, 2012.

[49] C. Sarkar and H. Hirani, "Synthesis and characterization of antifriction magnetorheological fluids for brake," *Def. Sci. J.*, vol. 63, no. 4, pp. 408–412, 2013.

[50] C. Sarkar and H. Hirani, "Theoretical and experimental studies on a magnetorheological brake operating under compression plus shear mode," *Smart Mater. Struct.*, vol. 22, no. 11, 2013.

[51] C. Sarkar and H. Hirani, "Design of a squeeze film magnetorheological brake considering compression enhanced shear yield stress of magnetorheological fluid," *J. Phys. Conf. Ser.*, vol. 412, no. 1, 2013.

[52] H. Shah and H. Hirani, "Online condition monitoring of spur gears," *Int. J. Cond. Monit.*, vol. 4, no. 1, pp. 15–22, 2014.

[53] K. P. Lijesh and H. Hirani, "Magnetic bearing using rotation magnetized direction configuration," *J. Tribol.*, vol. 137, no. 4, 2015.

[54] K. P. Lijesh and H. Hirani, "Modeling and development of RMD configuration magnetic bearing," *Tribol. Ind.*, vol. 37, no. 2, pp. 225–235, 2015.

[55] C. Sarkar and H. Hirani, "Synthesis and characterization of nano-particles based magnetorheological fluids for brake," *Tribol. Online*, vol. 10, no. 4, pp. 282–294, 2015.

[56] K. P. Lijesh and H. Hirani, "Optimization of Eight Pole Radial Active Magnetic Bearing," *J. Tribol.*, vol. 137, pp. 0245021–7, 2015.

[57] P. Kumar, H. Hirani, and A. Agrawal, "Scuffing behaviour of EN31 steel under dry sliding condition using pin-on-disc machine," *Mater. Today Proc.*, vol. 2, no. 4–5, pp. 3446–3452, 2015.

[58] C. Desai, H. Hirani, and A. Chawla, "Life Estimation of Hip Joint Prosthesis," *J. Inst. Eng. Ser. C*, vol. 96, no. 3, pp. 261–267, 2015.

[59] K. P. Lijesh and H. Hirani, "Design and development of Halbach electromagnet for active magnetic bearing," *Prog. Electromagn. Res. C*, vol. 56, pp. 173–181, 2015.

[60] K. P. Lijesh and H. Hirani, "Design of Eight Pole Radial Active Magnetic Bearing using Monotonicity," in *IcIIS Conference*, 2015, no. April.

[61] K. P. Lijesh and H. Hirani, "Development of analytical equations for design and optimization of axially polarized radial passive magnetic bearing," *J. Tribol.*, vol. 137, no. 1, pp. 1–10, 2015.

[62] C. Sarkar and H. Hirani, "Development of a magnetorheological brake with a slotted disc," *Proc. Inst. Mech. Eng. Part D J. Automob. Eng.*, vol. 229, no. 14, pp. 1907–1924, 2015.

[63] C. Sarkar and H. Hirani, "Synthesis and characterisation of nano silver particle-based magnetorheological fluids for brakes," *Def. Sci. J.*, vol. 65, no. 3, pp. 252–258, 2015.

[64] C. Sarkar and H. Hirani, "Effect of Particle Size on Shear Stress of Magnetorheological Fluids," *Smart Sci.*, vol. 3, no. 2, pp. 65–73, 2015.

[65] K. P. Lijesh and H. Hirani, "Failure mode and effect analysis of active magnetic bearings," *Tribol. Ind.*, vol. 38, no. 1, pp. 90–101, 2016.

[66] C. Sarkar and H. Hirani, "Experimental studies on Magnetorheological Brake containing Plane, Holed and Slotted Discs," *Ind. Lubr. Tribol.*, vol. 69, no. 2, 2016.